Eur. J. Mech., B/Fluids, **17**, n° 2, 145-164, 1998

Local and global instability properties of separation bubbles

D. A. HAMMOND and L. G. REDEKOPP

ABSTRACT. – A family of velocity profiles with reversed flow, typical of those found in separated flows, are examined for their linear instability properties. Specifically, a family of modified Falkner-Skan profiles are analyzed for the onset of absolute instability as the magnitude of the reversed flow increases. The mode of instability associated with the inflection point in the vicinity of the dividing streamline is found to become absolutely unstable as the peak reversed flow approaches about thirty percent of the free stream value. The family of profiles were used to construct generic models of separation bubbles and study the possible onset of global instability in the representative spatially-developing flows. © Elsevier, Paris.

1. Introduction

Flow separation in a streaming wall-bounded flow occurs frequently both in nature and in technological applications. For example, flow separation causes a precipitous loss of lift on an airfoil as the angle of attack reaches the critical or stall value. Separation bubbles appear spontaneously near the leading edge of airfoils, causing a dramatic increase in drag when the Reynolds number is decreased below a critical value depending on the angle of attack, airfoil thickness ratio, and leading-edge radius. Such closed separated regions with recirculating flow also occur near compression corners in supersonic flows, under the footprint of large amplitude waves, etc. Flow separation almost always has an adverse impact on performance and prediction of its onset and structure is of special concern to aerodynamicists and fluid dynamicists.

The existence of a local region of separated flow is intimately linked to the presence of streamwise gradients of such quantities as the impressed pressure field or the wall curvature. The structure of a separated region includes the existence of recirculating region where the mean motion is reversed relative to the oncoming stream. The point of origin of the reversed flow is termed the separation point, generally located on the wall, and the streamline emanating from this point and separating domains of reversed flow from the primary streaming flow is termed the dividing streamline. When the dividing streamline reattaches to the wall at a downstream position, a closed separation bubble is formed.

The present study is directed toward illuminating the instability characteristics of the spatially-nonuniform flow in a separation bubble. (Dovgal, Kozlow and Michalke, 1994) have recently discussed some local instability processes associated with separated flows, but our approach is quite different. We approach the problem from the viewpoint of local and global dynamics, seeking to provide some understanding of the possible modes of coherent, unsteady dynamics associated with such flows. In particular, we seek to provide qualitative insight to the conditions for the onset of local absolute instability in the generic kinds of reversed flow present in separated regions, and to explore the feasibility of the appearance of a global instability when the separation bubble exceeds a critical size. The presence of separation implies that reversed flow exists with an associated inflection point in the mean velocity profile which is positioned near the dividing streamline. It is known that when the

Department of Aerospace Engineering, University of Southern California, Los Angeles, California 90089-1191.

0997-7546/98/02/© Elsevier, Paris

backflow velocity in an isolated, free shear layer exceeds roughly fifteen percent of the speed of the primary stream, the inviscid mode of instability deriving from the inflectional profile will be of absolute type (*cf.* Huerre and Monkewitz, 1985). This means that a band of amplified waves exist in which some frequencies have group velocities directed upstream and some downstream. Now, the proximity of the wall to the inflection point in the velocity profile of a separating flow will clearly modify the condition for local absolute instability. As the size of a bubble grows, the peak backflow velocity can be expected to increase proportionately and conditions for local absolute instability are expected. The question of particular concern here is whether the backflow velocity magnitudes required for onset of absolute instability in a separating flow are attainable in realistic bubbles.

An issue closely linked to the appearance of local absolute instability in a spatially-developing flow is the onset of a global instability which organizes the flow over global scales, like the entire spatial extent of a separation bubble. It has been demonstrated in earlier studies by (Chomaz, Huerre and Redekopp, 1988, 1991) that, provided the region where local absolute instability exists is of sufficient streamwise extent, a global instability may ensue in which the entire spatial extent of the unstable region experiences a synchronous dynamics with strong streamwise coherence. The onset of such a global instability in most practical configurations will, of course, compete with the convected disturbances entering the separated region from the attached upstream boundary layer which serves as a spatial amplifier. Nevertheless, one may reason that the intrinsic frequency selection and modal structure of the possible global instability in the bubble will be uncoupled from the properties of the upstream amplifier. Since a global instability appears spontaneously and its characteristics are linked to the internal structure of the whole recirculating flow field in the bubble, it will likely dominate over any forcing by the upstream boundary layer. Of course, this is only speculative at the present stage. The work described here is a first step in determining whether one can reasonably expect the appearance of this type of global dynamics in separation bubbles.

This study was initially motivated by two practical circumstances where the issues discussed above are believed to be relevant. First, a recent data set (*cf.* Bogucki, Dickey and Redekopp, 1997) reveals surprisingly elevated levels of sediment resuspension occurring under the footprint of an isolated packet of long internal waves propagating against a long-shore current in coastal waters. The evidence shows that the upstream-propagating waves have amplitudes sufficient to create local separation bubbles in the boundary layer under the vertically-sheared current. The issue is that pronounced maxima are observed in resuspension of sedimentary material when the average surface stress (in the separated region) is lower than its nominal value in the region of attached flow. It is of considerable interest to identify the dynamical features inherent to the flow field in such separation bubbles which are responsible for stimulating the marked increase in potential for the flow to suspend particulate matter from the wall. Another motivation stems from a desire to suggest procedures for ameliorating the strong drag rise associated with the appearance of a leading-edge separation bubble forming on an airfoil at moderately-low Reynolds numbers (*cf.* Ward, 1963 and O'Meara and Mueller, 1987). The deleterious effect of such bubbles on airfoil performance begs for a control stimulus which can break up the bubble. Assuming the gravest global instability mode is lightly damped, so that the structure of the bubble remains robust in the presence of convected disturbances from the upstream boundary layer, one can envision injecting excitations from the wall under the bubble which can stimulate a consequent global instability of the sub-critical state. The resulting structure of the flow might, hopefully, lead to significant reductions in the drag. For these reasons and more, we embarked on a study of the stability properties of a family of reversed-flow velocity profiles to identify the potential for onset of global dynamics in separation bubbles.

2. Family of reversed-flow profiles

In our attemps to define conditions for appearance of local absolute instability in separated flows we have examined the instability properties of the Falkner-Skan family of velocity profiles (*cf.* Schlichting, 1968),

particularly along the branch with reverse flow, which are modified (or distorted) by an ad hoc structure function. Separated flow occurs for values of the Falkner-Skan pressure gradient parameter β in the range $-0.1988 < \beta < 0$ and the maximum reversed flow occurs for $\beta = -0.04$. To obtain velocity profiles where the strength of the backflow velocity and the depth of the reversed-flow portion of the profile could be varied independently, and over a considerably wider range than afforded by the Falkner-Skan family alone, the following three-parameter family of profiles was chosen

$$U(\eta) = f'(\eta; \beta) - a\eta e^{-(\eta-\eta_0)/\eta_0}, \tag{1}$$

where $f(\eta; \beta)$ is determined by the Falkner-Skan equation

$$f''' + ff'' + \beta[(1 - (f')^2] = 0; \quad f(0) = f'(0) = 0; \quad f'(\infty) = 1. \tag{2}$$

(a)

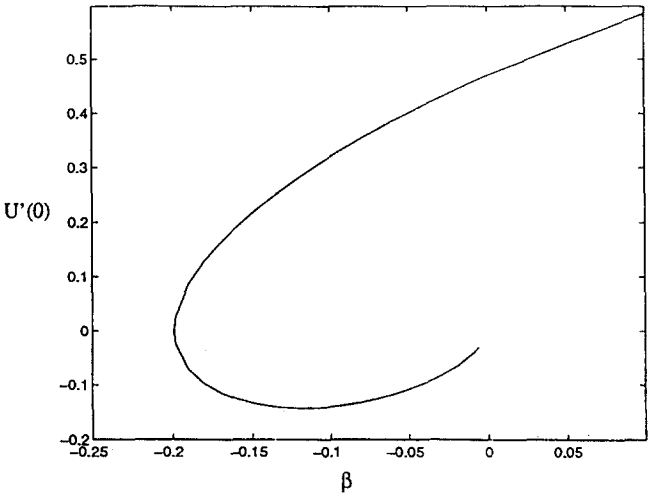

(b)

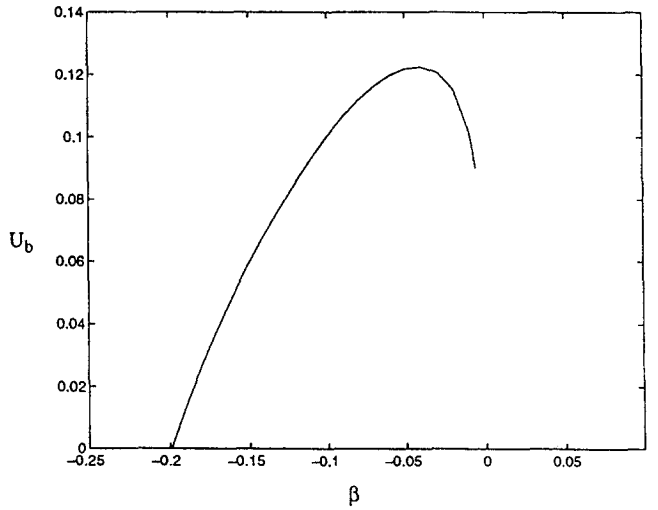

Fig. 1. – Variation of the (a) wall shear and (b) peak backflow velocity for the separated flow branch of Falkner-Skan solutions.

Primes denote derivatives with the (cross-stream) similarity variable η. The perturbation parameter a serves to augment the wall-shear of the separated flow (and, thereby, the strength of the backflow relative to the separated Falkner-Skan value at a given β) and η_0 allows variation of the thickness of the reversed flow portion (and, to some extent, the slope of the profile at the inflection point associated with the internal shear layer around the dividing streamline). In what follows, we "unlook" the parameter β from the true pressure gradient and simply use it as a profile parameter which is useful in prescribing the shape of local velocity profiles in a separating flow. This approach is somewhat analogous to that employed by Lees and Reeves (1994) in their analysis of shock separated flows in laminar boundary layers by integral methods.

Some of the characteristics of the above family of profiles are shown in Figures 1 and 2. Figure 1 displays, for reference purposes, the wall shear and the maxium backflow velocity U_b (U_b is positive for reverse flow) for the Falkner-Skan family (*i.e.*, with perturbation parameter $a = 0$). The backflow applies only for the reverse flow portion where $-0.1988 < \beta < 0$ and $U'(\eta = 0) < 0$. The wall shear for the perturbed family varies linearly with the perturbation parameter a

$$U'(0) = f''(0; \beta) - ae^1. \tag{3}$$

(a)

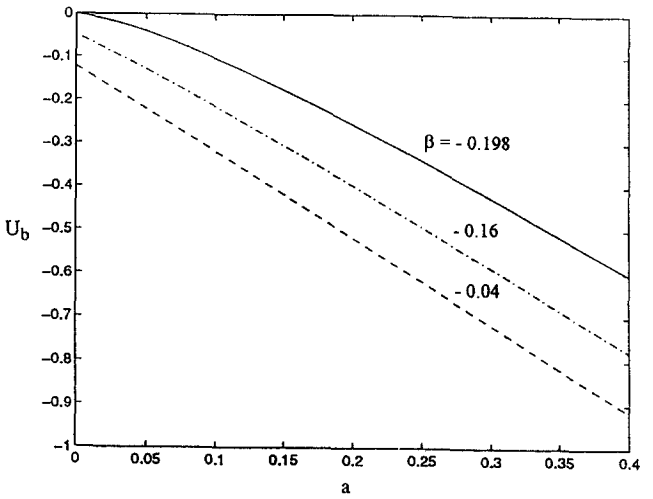

(b)

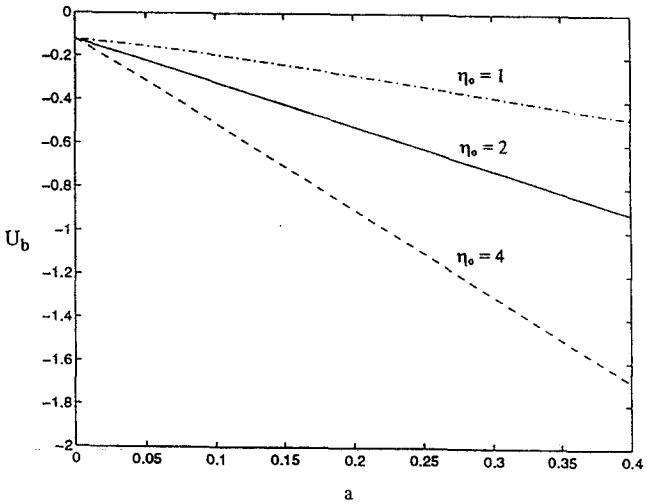

Fig. 2. – Peak backflow velocities for the perturbed family of separated flow profiles.
(a) The effect of β for $\eta_0 = 2$. (b) The effect of η_0 for $\beta = -0.04$.

The maximum backflow U_b on the other hand varies with all three parameters of the family β, a, η_0. Figure 2 exhibits this backflow as a function of the parameter a for selected values of β and η_0. It is apparent that U_b increases nearly linearly with a for $\beta = -0.04$ where the Falkner-Skan family gives a maximum value for U_b.

Other characteristics of these profiles which are relevant to the later discussion of separation bubbles are the height of the reversed flow region η_{ds} (or, the position of the dividing streamline in the case of a bubble) and the displacement thickness δ^*. The location of the dividing streamline η_{ds} is shown in Figure 3. As expected, η_{ds} varies quite strongly for the Falkner-Skan family, especially near the separation value $\beta = -0.1988$, and is most sensitive to the value of the perturbation parameter a near this value of β. The displacement thickness for the pertubed family is readily found to vary linearly with a and quadratically with η_0,

$$\delta^* = \int_0^\infty \{1 - U(\eta)\}\, d\eta = \delta^*_{FS}(\beta) + a\eta_0^2\, e^1, \tag{4}$$

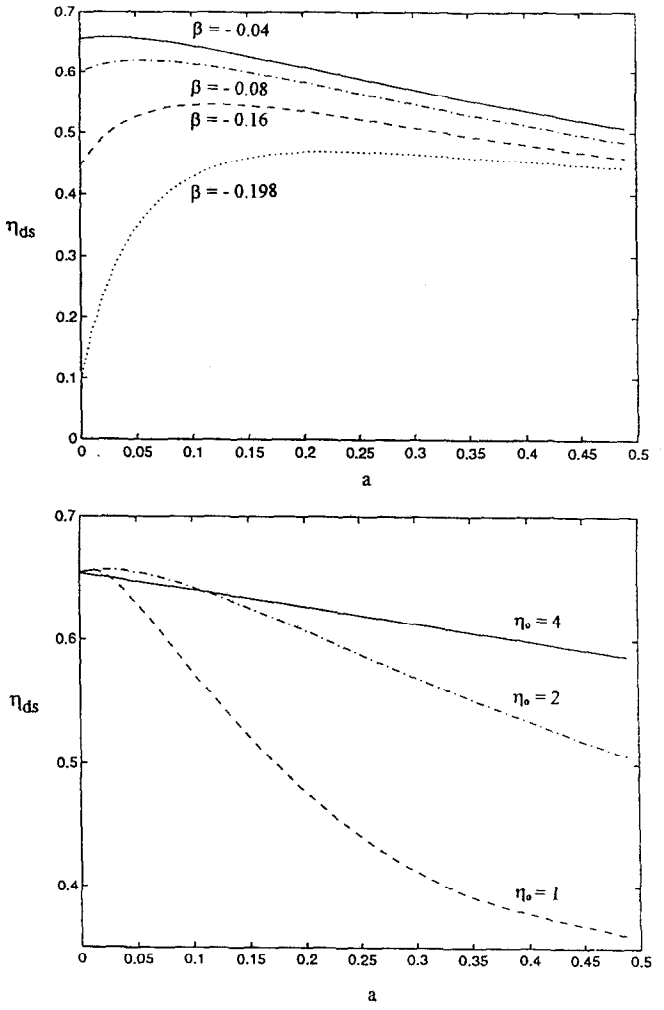

Fig. 3. – Variation of the dividing streamline position η_{ds} with the perturbation parameter a. (a) The effect of β for $\eta_0 = 2$. (b) The effect of η_0 for $\beta = -0.04$.

The quantity $\delta^*_{FS}(\beta)$ is the displacement thickness of the Falkner-Skan profile at prescribed β and numerical values for negative β along both the attached and separated branches are given in Table I.

TABLE I. – Displacement function data for the Falkner-Skan family with negative β.

Attached flow		Separated flow	
β	δ^*	β	δ^*
0.0	1.218	–0.198	2.388
–0.02	1.253	–0.18	3.085
–0.04	1.292	–0.16	3.529
–0.06	1.336	–0.14	3.954
–0.08	1.386	–0.12	4.400
–0.10	1.444	–0.10	4.896
–0.12	1.512	–0.08	5.480
–0.14	1.597	–0.06	6.220
–0.16	1.708	–0.05	6.689
–0.18	1.873	–0.04	7.272
–0.198	2.333	–0.03	8.042

3. Instability properties

The linear instability properties of the family of perturbed Falkner-Skan profiles were determined by numerical solution of the Orr-Sommerfeld equation (*cf.* Drazin and Ried, 1981)

$$(5)\qquad \begin{cases} \phi'''' - 2\alpha^2\phi'' - \alpha^4\phi = i\alpha\,\mathrm{Re}\left\{\left(U - \dfrac{\omega}{\alpha}\right)(\phi'' - \alpha^2\phi) - U''\phi\right\}, \\ \phi(0) = \phi'(0), \quad \lim_{Y\to\infty} \phi,\ \phi' = 0. \end{cases}$$

The eigenfunction $\phi(Y)$ is proportional to the amplitude of the transverse velocity component of a normal mode disturbance of the form $\exp\{i(\alpha x - \omega t)\}$. Primes in this equation denote differentiation with respect to the independent variable $Y = \eta/\delta^*$. The velocity profile $U(Y)$, defined by (1) in terms of the rescaled variable Y, is assumed to represent a parallel shear flow. In this framework, the equation is made dimensionless using the displacement thickness δ^* as the length scale and the free stream velocity U_∞ as the velocity scale. Hence, the Reynolds number Re appearing in (5) is based on U_∞ and δ^*, as are the frequency ω and wavenumber α of a monochromatic disturbance which is superposed on the assumed parallel flow. Equation (5) defines an eigenvalue problem with complex eigenfunction $\phi(Y)$ and yields the dispersion relation

$$(6)\qquad D(\omega, \alpha; \mathrm{Re}, \beta, a, \eta_0) = 0$$

relating complex values of ω and α. In particular, the absolute frequency $\omega_0 = \omega(\alpha_0; \mathrm{Re}, \beta, a, \eta_0)$ can be computed where α_0 is specified by requiring the group velocity to vanish

$$(7)\qquad \left.\frac{\partial\omega}{\partial\alpha}\right|_{\alpha_0} = 0.$$

This allows calculation of the absolute growth rate $\omega_{0_i} = \Im\{\omega_0\}$ and the conditions for the onset of local absolute instability $\omega_{0_i} > 0$. In practice, the value of ω_0 was determined by examining the images in the complex α-plane of the trajectories $\omega_i = \Im\{\omega\} =$ constant in the complex ω-plane. The value of ω leading to incipient pinching of the upstream and downstream spatial branches of the dispersion relation determines ω_0.

Our numerical procedure for solution of the eigenvalue problem (5) was tested for the Falkner-Skan profiles. Values of the critical Reynolds number of Re = 522, 318, and 199 for $\beta = 0, -0.05, -0.1$, respectively, along the branch of attached boundary layers, agrees precisely with those reported by Wazzan, Taghavi and Keltner (1974). Values of the temporal growth rate for the Blasius boundary layer differ by less than one percent from those reported by Gaster and Jordinson (1975).

For reference purposes, the absolute growth rate for the unperturbed Blasius boundary layer ($\beta = a = 0$) was computed first. Results are shown in Figure 4. Consistent with results reported by Gaster and Jordinson (1975), the Blasius boundary layer is convectively unstable at all Reynolds numbers. The branch point values we compute $\omega_0 = 0.022055 - 0.034604i$, $\alpha_0 = 0.074403 - 0.057624i$) at Re = 1000 are within about five percent of those reported by Gaster and Jordinson ($\omega_0 = 0.020488 - 0.032855i$, $\alpha_0 = 0.079878 - 0.059820i$). Eigenvalues were computed using a shooting method and a pseudo-orthogonalization technique similar to that proposed by Monkewitz (1978). For several parameter conditions, the eigenvalues computed by this method were compared with those obtained using another solver based on the Riccati method described by Davey (1973, 1977, 1979). Excellent agreement was found in each case where results from the two solvers were compared.

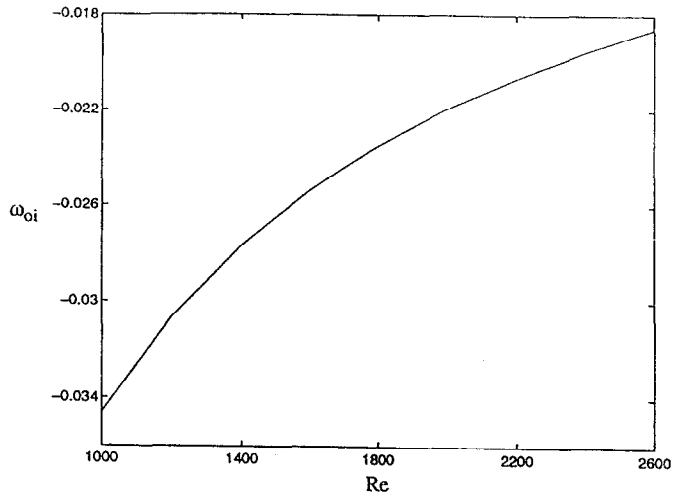

Fig. 4. – Variation of the absolute growth rate with Reynolds number for the Blasius boundary layer ($\beta = a = 0$).

Although the variation of the absolute growth rate shown in Figure 4 is seen to be increasing with increasing Reynolds number, it is apparent that ω_{0_i} remains negative for all Reynolds numbers. When the variation of the absolute growth rate, for fixed Reynolds number, is considered for negative values of the pressure gradient parameter β along the reversed flow branch of the Falkner-Skan solutions, two modes of instability appear. One, here termed the viscous or wall mode, is a continuation of the Blasius mode and the other, termed the inviscid or shear layer mode, arises from the existence of an inflection point associated with the presence of reversed flow. The absolute growth rates for the viscous mode alone is shown in Figure 5 for two different Reynolds numbers. The lower portion of each curve applies to the case of attached flow and the upper portion to separated flow. The two portions of each curve merge at the condition for incipient reversed flow, namely $\beta = -0.1988$.

The distribution of absolute growth rates as a function of β for the inviscid mode alone is shown in Figure 6 for Re = 1000. Of course, this mode only exists for separated flow. The maximum value of ω_{0_i} is realized for $\beta = -0.02$, even though the reversed flow is at least ten percent smaller at $\beta = -0.02$ than at $\beta = -0.04$. The explanation for this result lies in the fact that the inflection point at $\beta = -0.02$ is displaced farther from the

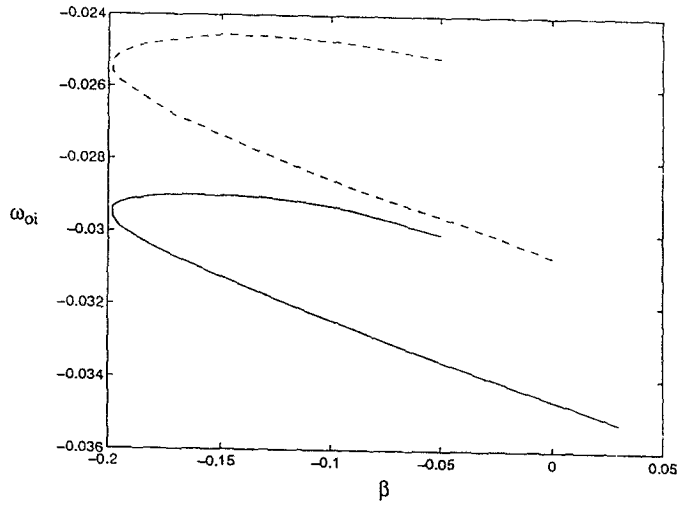

Fig. 5. – Variation of the absolute growth rate with pressure gradient parameter β for the Falkner-Skan family for Re = 1000 (——) and Re = 1200 (– – –).

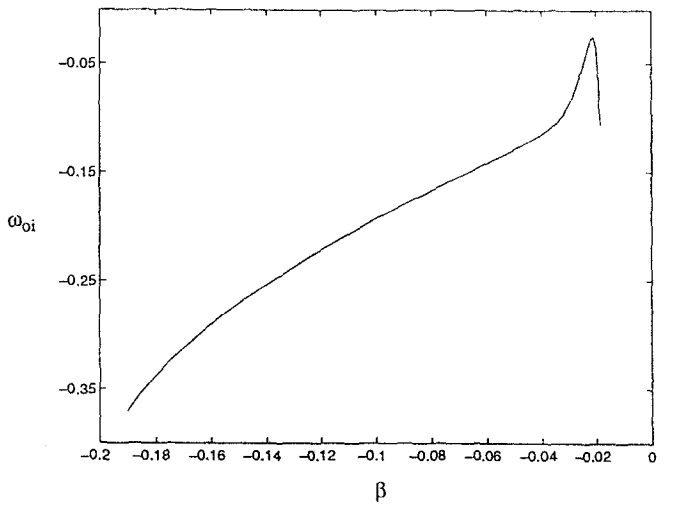

Fig. 6. – Variation of the absolute growth rate with β for the inviscid mode of the Falkner-Skan family ($a = 0$) of separated flows for Re = 1000.

wall when compared to its position for $\beta = -0.04$. The no-slip constraint on the disturbance velocity affects the group velocity of an instability mode associated with the shear layer located near the dividing streamline. This effect of the presence of a wall in proximity of a mixing layer was investigated further for a generic profile, namely the hyperbolic-tangent mixing layer profile, and results are given in the Appendix. It is shown there that, when the magnitude of the reversed flow is held fixed and a wall is moved toward the inflection point, the flow becomes more convectively unstable. In other words, the presence of a wall on the low-speed side of a mixing layer requires an increased amount of backflow for the mixing layer to become absolutely unstable when compared to the unbounded mixing layer. Representative forms of the spatial branches for the Falkner-Skan family in the vicinity of the pinching point for both the inviscid and viscous branches are shown in Figure 7.

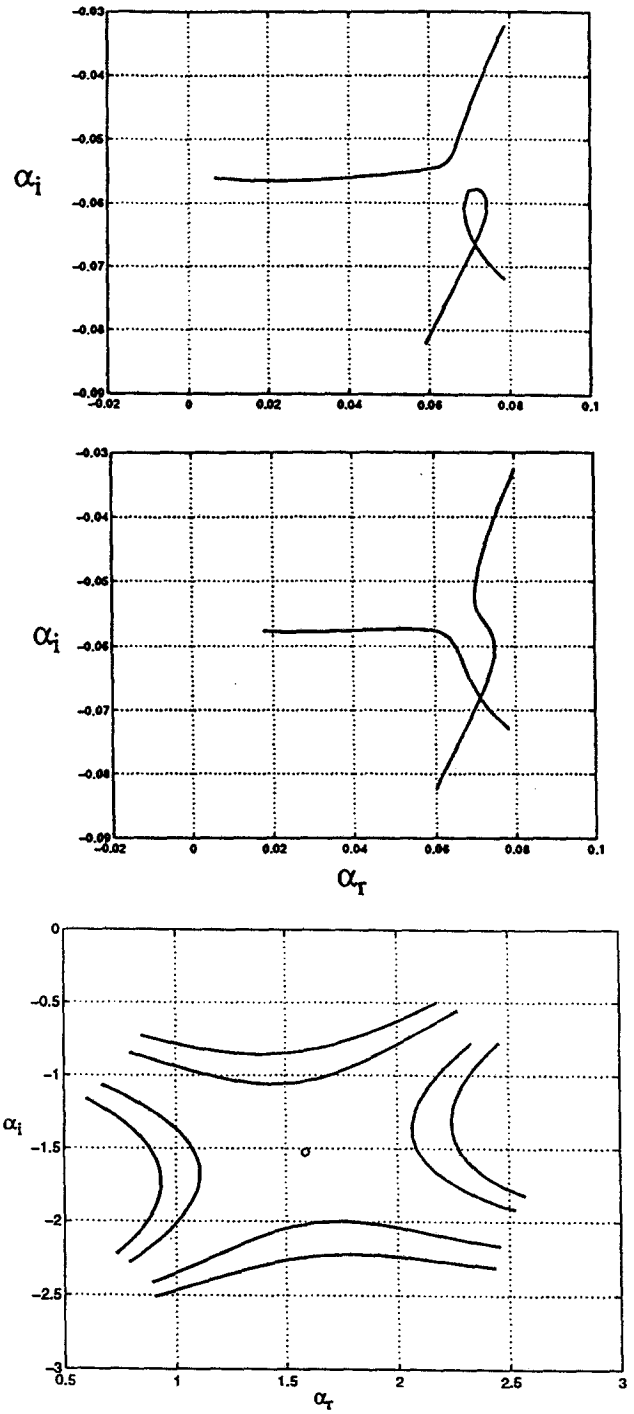

Fig. 7. – Representative spatial branches of the Falkner-Skan family ($a = 0$) of separated flows for Re $= 1000$. (a) The viscous mode for $\beta = -0.09$ with $\omega_0 = 0.01865 - 0.03265i$, $\alpha_0 = 0.06736 - 0.005631i$. Branches shown correspond to $0 < \omega_r < 0.024$ and $\omega_i = -0.0324$ in the top panel and $\omega_i = -0.0328$ in the lower panel. (b) The inviscid mode for $\beta = -0.11$ with $\omega_0 = 0.614 - 0.207i$, $\alpha_0 = 1.588 - 1.526i$. Branches shown correspond to $0.4 < \omega_r < 0.9$ and $\omega_i = -0.11, -0.16, -0.26, -0.31$.

A sequence of calculations were performed using the perturbed family of velocity profiles (1) to determine the conditions for the onset of absolute instability in a broader class of separated flow. A partial summary of the results is shown in Figure 8. Figure 8a displays the boundary between absolute and convective instability for the inviscid mode in the a-η_0 plane for two different values of the Falkner-Skan parameter β and at fixed Reynolds number. The fact that the transition boundaries intersect for different values of β is associated with the variation of the backflow velocity and the position of the inflection point as the perturbation parameters (a, η_0) are varied for the given values of β. Figure 8b defines the dimensionless backflow velocity required to achieve the transition from convective to absolute instability shown in Figure 8a. The critical values of backflow velocity for the two choices of β are now distinct for low values of η_0 and reach similar asymptotic values as η_0 becomes large. It is evident that the required strength of the reversed flow increases dramatically as η_0 decreases. This occurs because of a subtle interplay between the strength of the backflow velocity and the location of the inflection point as either parameter is varied while holding the other perturbation parameter fixed. As η_0 becomes large, the affect of β on the critical backflow velocity is considerably reduced because

(a)

(b)

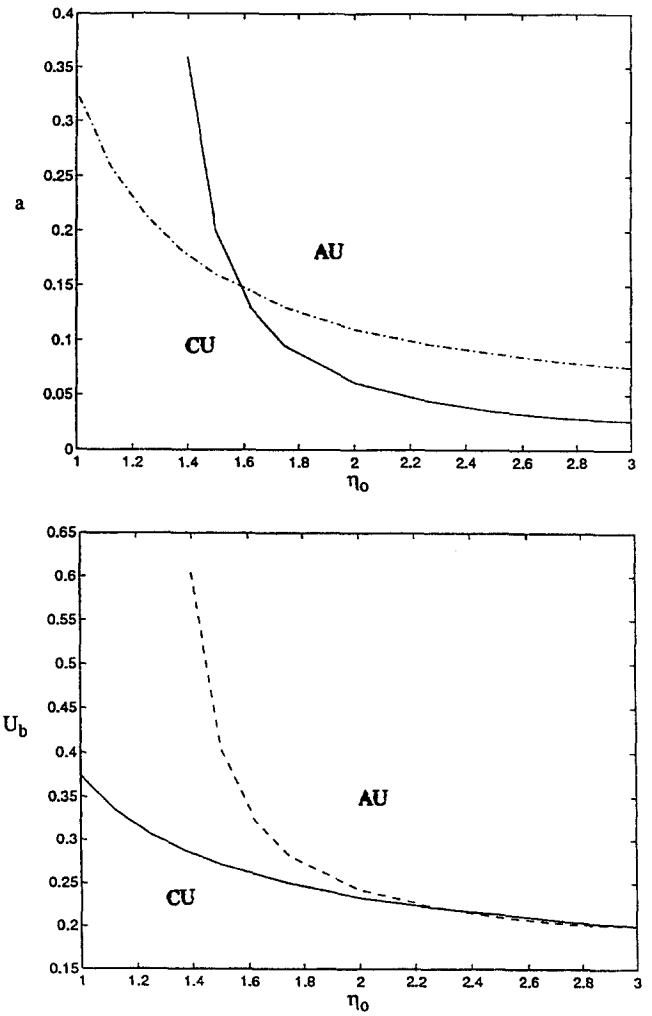

Fig. 8. – Absolute-convective instability transition boundaries for the perturbed family of velocity profiles for $\beta = -0.04$ (– – –) and $\beta = -0.16$ (——). (a) Transition boundary in (a, η_0) plane. (b) Peak backflow velocity corresponding to the transition boundary shown in (a).

the inviscid instability associated with the inflection point becomes independent of the details of the profile near the wall. In the limit as η_0 increases, the inflectional instability seems to approach a value not much higher than that of a free mixing layer. Using a hyperbolic-tangent function for the mixing-layer velocity profile and taking $\mathrm{Re} \to \infty$, Huerre and Monkewitz (1985) showed tha the critical backflow velocity was $U_b = 0.136$. In the present case, an approximate critical value of $U_b \simeq 0.2$ is obtained as $\eta_0 \to \infty$ using the perturbed Falkner-Skan profile and $\mathrm{Re} = 1000$.

4. Results for a model separation bubble

A model for the spatially-developing flow in a separation bubble was constructed using the perturbed Falker-Skan family (1) where the parameters β, a, and η_0 are allowed to vary with the streamwise position x. Clearly, there is considerable arbitrariness in the specification of the bubble shape and the flow characteristics within the bubble. Furthermore, the nonparallel nature of the base flow will not be accurately represented by use of a locally parallel flow assumption in the instability analysis when the streamwise gradients of mean velocity are not extremely weak. The latter effect is ignored in this more qualitative study of the stability properties of separation bubbles. Our goal is quite simply to gain some insight concerning the typical strength of backflow required in "reasonable" bubble shapes in order to achieve local absolute instability, and to provide some qualitative feel for conditions necessary for onset of a confined global instability. Hence, we chose to specify a simple, symmetric dividing streamline shape $\eta_{ds}(x)$ using the center plane of the bubble as the reference position $x = 0$. We also require that all flow properties, like the peak backflow velocity at any position and the wall shear stress at that position, attain local extrema at the bubble symmetry position $x = 0$, and vary smoothly (*i.e.*, monotonically) as one moves away from the bubble center. We do not claim, therefore, that the results presented here apply quantitatively to any specific computed or measured separated flow bubble, but only that these results provide a useful and reasonable guide for assessing the conditions when incipient absolute instability may be expected locally in a separation bubble. Parenthetically, we note here that specific separation bubbles induced by an upstream-propagating Korteweg-deVries solitary wave in a shallow-water mean shear flow, and their instability properties, is in progress in a separate effort. Our purposes here are quite general and not tied to specific separated flows. The goal is to provide qualitative guidelines for assessing critical conditions in a general class of separated flows.

We consider a family of separation bubbles having dividing streamlines in the shape of circular arcs

$$\eta_{ds}(x) = \eta_m \left(1 - 4\frac{x^2}{c^2}\right). \tag{8}$$

The aspect ratio of the bubble is given by η_m/c, where η_m specifies the maximum displacement of the dividing streamline at the center position $x = 0$. The velocity profiles at the extremities $x = \pm c$ of the bubble are the Falkner-Skan family ($a = 0$) with $\beta = -0.1988$, where U_b and the wall shear both vanish. For $-c < x < +c$, the backflow velocity is positive and the wall shear stress is negative, both varying monotonically from the extremities of the bubble toward the center.

We present here two specific examples of bubbles where the parameter η_0 is fixed at $\eta_0 = 2$ and the length of the separated region is fixed with $c = 15$, leading to a separated region of length $L_s = 2c = 30$. The aspect ratio of the bubbles are both close to 50, but different distributions $a(x)$ and $\beta(x)$ are used to define the flow characteristics in the bubble. The resulting distributions of the backflow velocity, the wall shear stress, the displacement thickness, and the computed absolute growth rate for these two bubbles are shown in Figure 9.

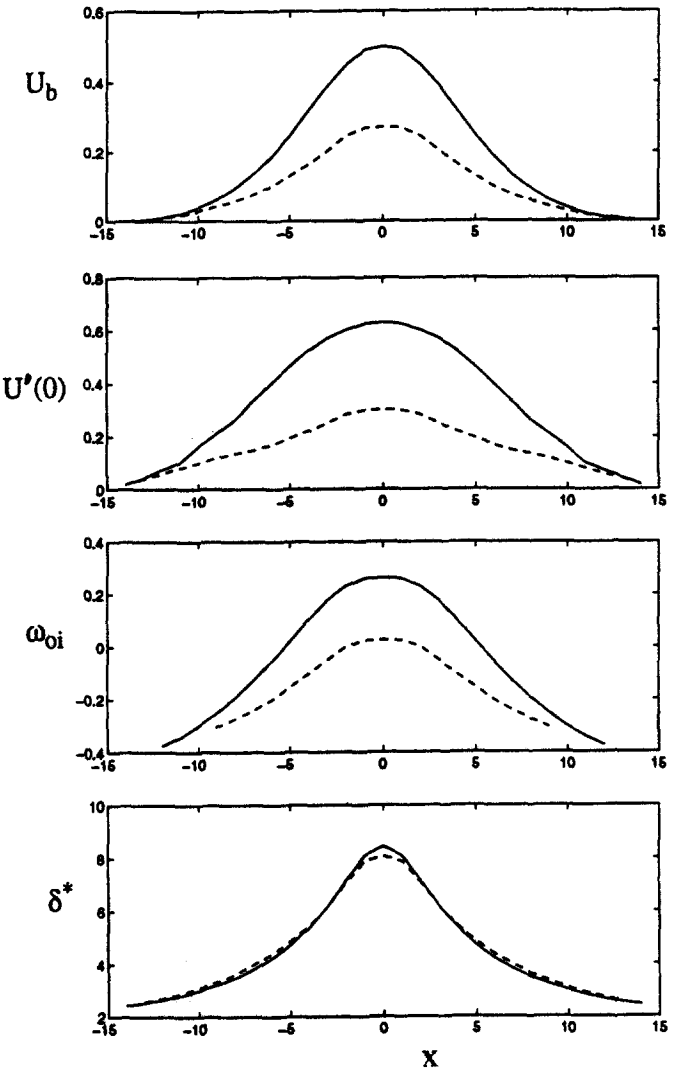

Fig. 9. – Distributions of peak backflow velocity, wall shear $U'(0)$, absolute growth rate, and displacement thickness for two model separation bubbles. Bubble A (– – –); Bubble B (——).

The bubble shape with the lowest peak backflow velocity (Bubble A) is seen to be only slightly absolutely unstable over a central region of roughly five spatial units. This is achieved with a maximum backflow velocity of $U_b = 0.270$ occurring at the center of the bubble $x = 0$. The maximum (negative) wall shear stress associated with the reversed flow in the bubble is –0.301 compared to the nominal Blasius value of $0.469 = 0.0332\sqrt{2}$. Slightly decreased magnitudes of the wall shear stress would exist if the parameter η_0 would be increased near the bubble center. Based on the results shown in Figure 8, this would also allow the onset of local absolute instability with slightly smaller peak backflow velocities. We find, therefore, that local absolute instability in spatially-developing flows typical of separation bubbles can be realized with quite moderate backflow velocities. The other hypothetical bubble (Bubble B) was constructed with somewhat steeper streamwise gradients in the wall shear stress and having stronger, but not unreasonably high, values of peak backflow velocities. A scaled schematic of Bubble B with local velocity profiles is shown in Figure 10. Since the bubble is symmetric, profiles

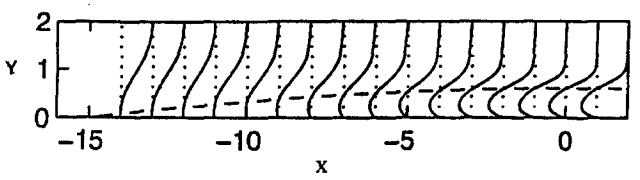

Fig. 10. – Velocity profiles and dividing streamline shape for Bubble B.

are shown only for the upstream half of the bubble. The peak absolute growth rate, and the streamwise extent over which it is positive, are significantly increased relative that for Bubble A.

Based on the results for these two sample separation bubbles, it seems reasonable to hypothesize that separation bubbles may well realize regions of local absolute instability near their centers, especially if the peak backflow velocity approaches thirty percent of the free stream value. With the existence of absolute instability in the central region, a bubble is likely to be susceptible to intrinsic dynamics that can potentially overwhelm any convectively unstable disturbances entering the bubble from the attached boundary layer upstream of the separation.

5. Global instability analysis

An approximate analytical approach is employed to assess whether the sample bubbles presented above are unstable to a global, or streamwise, eigenmode. A linear evolution model for the streamwise structure of a possible global instability is developed based on the following truncated approximation of the dispersion relation

$$\omega = \omega_0 + \frac{1}{2}\omega_{\alpha\alpha}(\alpha - \alpha_0)^2. \tag{9}$$

The parameters in this relation are the absolute frequency ω_0, associated wave number α_0 defined in (7), and the curvature of the dispersion relation $\omega_{\alpha\alpha}$. Consistent with WKBJ theory, we assume that the parameters vary in the streamwise direction on the slow scale $X = \varepsilon x$. The linear evolution equation consistent with the dispersion relation (9) can then be expressed in the form

$$i\left(\frac{\partial A}{\partial t} - \alpha_0(X)\,\omega_{\alpha\alpha}(X)\,\frac{\partial A}{\partial x}\right) + \frac{1}{2}\omega_{\alpha\alpha}(X)\,\frac{\partial^2 A}{\partial x^2} - \left\{\omega_0(x) + \frac{1}{2}\alpha_0^2(X)\,\omega_{\alpha\alpha}(X)\right\} A = 0. \tag{10}$$

In this reduced model we focus exclusively on the streamwise development of the disturbance field, completely suppressing any dependence on the cross-stream or eigenfunction direction. A consistent asymptotic reduction of the equations of motion for an unstable wave mode in a spatially-developing flow, leading to (10), has been provided by Monkewitz, Huerre and Chomaz (1993).

A global mode in the present context is a solution of (10) having the form

$$A(x, t; \varepsilon) = \Phi(X; \varepsilon)\, e^{-i\omega_g t}, \tag{11}$$

where ω_g is the global mode frequency. If $\Im\{\omega_g\} > 0$, the global mode is unstable. The modal eigenfunction $\Phi(X; \varepsilon)$ which defines the streamwise structure of the disturbance field associated with a global instability satisfies homogeneous boundary conditions, like the vanishing of the disturbance field at a rigid boundary or asymptotically provided the flow is stable at $x = \pm\infty$. Chomaz, Huerre and Redekopp (1991) employed the

linear, variable-coefficient, Ginzburg-Landau equation (10) to determine generic criteria for the onset of a global instability and its frequency selection. In particular, they demonstrated that the saddle point position defined by

$$\left.\frac{\partial \omega_0}{\partial X}\right|_{X_s} = 0, \tag{12}$$

where X_s is in general complex, is the appropriate position about which the variable coefficients in (10) should be referenced. They also showed that the leading-order estimate for the frequency of oscillation of the gravest global mode is given by $\Re\{\omega_0(X_s)\}$.

The eigenvalue problem for the global mode solution of (10) can be reduced to the solution of

$$\frac{d^2\phi}{dX^2} + \left[\frac{2(\omega_g - \omega_0)}{\varepsilon^2 \omega_{00}} + \frac{i}{\varepsilon}\alpha_0'(X)\right]\phi = 0, \tag{13}$$

where we have used the transformation

$$\Phi(X;\varepsilon) = \phi(X;\varepsilon)\exp\left\{\frac{i}{\varepsilon}\int_{X_s}^{X} \alpha_0(X')\,dX'\right\}. \tag{14}$$

The saddle-point position X_s for the spatially-symmetric separation bubbles considered in the previous section occurs at $X_s = 0$, since we have chosen to study exclusively the class of symmetric separation bubbles. The boundary conditions for a global mode solution require ϕ to vanish far upstream and far downstream. The global mode eigenfunction is then centered in the region of absolutely unstable flow (*i.e.*, the separation bubble) and decays uniformly in the region of convectively unstable flow. In this case, we are not considering forced global mode solutions stimulated by convected disturbances coming from upstream.

Referring to the two bubble configurations shown in Figure 9, several analytical approximations for the symmetric distributions of $\omega_0(X)$ and $\alpha_0(X)$ can be proposed. Since we suppose that the attached boundary layers upstream of separation and downstream of reattachment approach convectively unstable (or stable) flows like the Blasius boundary layer, one could propose a "global" representation of the following form for both the real and imaginary parts of $\alpha_0(X)$:

$$\alpha_0(X) = \alpha_{00} + (\alpha_{00} - \alpha_{0\infty})\,\mathrm{sech}^2\left(\frac{X}{X_\alpha}\right), \tag{15}$$

where $\alpha_{00} = \alpha_0(0)$ and $\alpha_{0\infty} = \lim_{x\to\pm\infty}\alpha_0(X)$. The scale parameter X_α can be determined directly from the curvature of $\alpha_0(X)$ at the center of the separation bubble. Entirely similar forms for the real and imaginary parts of $\omega_0(X)$ can be proposed. Alternately, one could seek a "local" representation of the form

$$\begin{cases} \alpha_0(X) = \alpha_{00} + \dfrac{1}{2}\alpha_{0_{XX}}X^2, \\ \omega_0(X) = \omega_{00} + \dfrac{1}{2}\omega_{0_{XX}}X^2, \end{cases} \tag{16}$$

in which all aspects of the approximate distributions are related to properties at the saddle point ($X_s = 0$). The latter forms are convenient in that they allow a straightforward analytical solution of the eigenvalue problem in (13). Relevant data for these analytic representations for the two separation bubbles are given in Table II.

TABLE II. – Data for separation bubbles.

	Bubble A	Bubble B
ω_{00}	$0.73606 + 0.02580i$	$0.49171 + 0.26194i$
ω_{0_∞}	$0.02206 - 0.03460i$	$0.02206 - 0.03460i$
$\omega_{\alpha\alpha}$	$-0.00022 - 0.46500i$	$-0.09180 - 0.37900i$
$\omega_{0_{xx}}$	$-0.02922 - 0.00168i$	$-0.02868 - 0.00456i$
α_{00}	$1.91097 - 1.55479i$	$2.11517 - 1.19442i$
$\alpha_{0_{xx}}$	$-0.00314 + 0.04658i$	$-0.00884 + 0.08134i$
α_{0_∞}	$0.07440 - 0.05762i$	$0.07440 - 0.05762i$
x_α	$34.20000 + 8.01800i$	$21.49000 + 5.28700i$
x_ω	$6.9918 + 8.47970i$	$5.7229 + 8.06416i$

Considering first the "local" representation given in (16), and assuming $\omega_{\alpha\alpha} = \omega_{\alpha\alpha}(0) =$ constant, (13) reduces to Hermite's equation and the discrete eigenvalues for the global mode frequencies are

$$\omega_{g_n} = \omega_{00} + \omega_{\alpha\alpha}\sqrt{\frac{\omega_{0_{XX}}}{\omega_{\alpha\alpha}}}\left(n + \frac{1}{2}\right) + \varepsilon^2 \frac{(\alpha_{0_{XX}}\,\omega_{\alpha\alpha})^2}{\omega_{0_{XX}}}, \quad n = 0, 1, 2, \ldots \tag{17}$$

This expression reveals that, to leading order, the frequency of the global mode is given by the real part of the absolute frequency at the saddle point, the result first predicted by Chomaz, Huerre & Redekopp (1991). The corresponding eigenfunction $\phi(X;\varepsilon)$ for the gravest mode is

$$\phi_0(X;\varepsilon) \propto \exp\left\{-\frac{X^2}{2\varepsilon}\sqrt{\frac{\omega_{0_{XX}}}{\omega_{\alpha\alpha}}} - \frac{iX}{2}\,\alpha_{0XX}\sqrt{\frac{\omega_{\alpha\alpha}}{\omega_{0_{XX}}}} + \frac{\varepsilon}{8}\,\alpha_{0XX}^2\sqrt[3]{\frac{\omega_{\alpha\alpha}}{\omega_{0_{XX}}}}\right\}. \tag{18}$$

This expression, combined with the exponential factor in (14), defines the streamwise structure of the disturbance field in the separation bubble. Using the relevant data summarized in Table II for the two separated flow regions, the following global mode eigenfrequencies are computed:

$$\begin{aligned}
&\text{Bubble A:} \quad \omega_{g_0} = 0.7218 - 0.0068i,\\
&\qquad\qquad\ \ \omega_{g_1} = 0.7255 - 0.0697i,\\
&\text{Bubble B:} \quad \omega_{g_0} = 0.4206 + 0.2400i,\\
&\qquad\qquad\ \ \omega_{g_1} = 0.3424 + 0.1678i,\\
&\qquad\qquad\ \ \omega_{g_2} = 0.2642 + 0.0957i,\\
&\qquad\qquad\ \ \omega_{g_3} = 0.1860 + 0.0235i,\\
&\qquad\qquad\ \ \omega_{g_4} = 0.1078 - 0.0487i.
\end{aligned} \tag{19}$$

It is apparent that Bubble A is only marginally stable on a global basis and that Bubble B is strongly unstable. It is also apparent that globally unstable modes exist for Bubble B. One expects the gravest mode to dominate, but nonlinear interactions may give rise to quite different global dynamics, especially if resonances occur.

Global mode eigenfrequencies were also computed using distributions of the form (15) for the real and imaginary parts of $\omega_0(X)$ and $\alpha_0(X)$. The numerical results in this case are as follows:

$$\begin{aligned}
&\text{Bubble A:} \quad \omega_{g_0} = 0.620 - 0.088i,\\
&\qquad\qquad\ \ \omega_{g_1} = 0.541 - 0.154i,\\
&\text{Bubble B:} \quad \omega_{g_0} = 0.455 + 0.228i,\\
&\qquad\qquad\ \ \omega_{g_1} = 0.390 + 0.160i.
\end{aligned} \tag{20}$$

The global stability or instability for the bubbles determined analytically using the simple "local" approximations (16) for $\omega_g(X)$ and $\alpha_0(X)$ is sustained, although some quantitative differences do exist in the frequencies and growth rates for the different modes. It seems quite clear, at least for the model symmetric separation bubbles examined here, that global instability should be expected when the strength of the reversed flow with in the bubble approaches (roughly) 30% of the ambient stream speed.

The structure of these bubbles is such that local flow states are unstable, either absolutely or convectively, but the entire spatially-developing flow is only globally unstable if the internal pocket of local absolute instability exceeds a critical size. The eigenstructure of the gravest global mode for Bubble A, computed using the local approximation and (18), is shown in Figure 11. This mode was selected because it is nearly neutral and nonlinear effects are likely to be negligible. The reader will note that results in Figure 11 are presented in terms of the "fast" x coordinate and that the separation bubble has streamwise extent $-15 < x < 15$. The eigenfunction was computed using the "global" representation (15) for $\alpha_0(X)$ in the exponential factor in (14) together with the expression (18) for $\phi_0(x)$. This was done to avoid the unphysical effect on the eigenstructure when the "local" variation of $\alpha_0(X)$ in (16) is substituted into the integral quantity appearing in the exponential factor of (14). The eigenfunction depicted in Figure 11 was normalized such that the peak value of $|\Phi(x)|$ was unity.

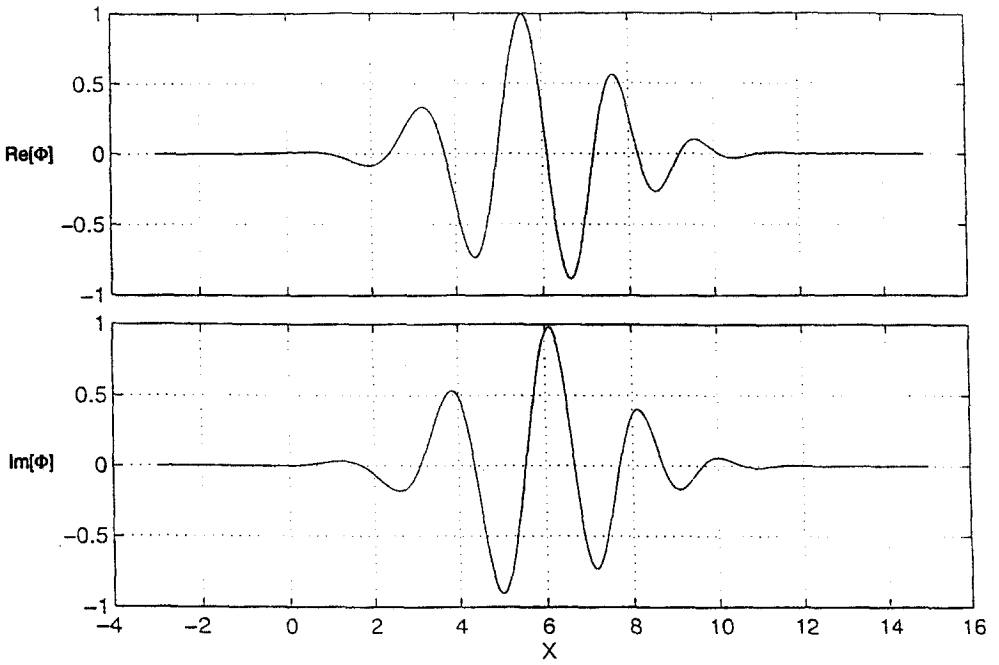

Fig. 11. – Global mode eigenfunction for Bubble A (local representation of $\alpha(X)$ and $\omega_0(X)$).

The eigenfunction for the same mode obtained by using the global representation (15) for $\alpha_0(X)$ and $\omega_0(X)$ is shown in Figure 12. The model shape is clearly modified by the different spatial distributions of $\alpha_0(X)$ and $\omega_0(X)$, being somewhat asymmetric and slightly broader when the "global" distributions are used, but the wavelength is quite comparable in either case. The downstream shift of the peak of the eigenfunction from the position where ω_{0i} has a local maxima was previously noted by Chomaz, Huerre, and Redekopp (1990) in another context. This shift comes about from the $\partial A/\partial X$ term in (10) which breaks the $X \rightarrow -X$ symmetry when the coefficients are constant or are given by symmetric functions of X.

The significance of the existence of a (linearly unstable) global mode is that it imposes a marked reduction in the streamwise length scale of the flow in a separation bubble, leading to a spatially coherent structure within

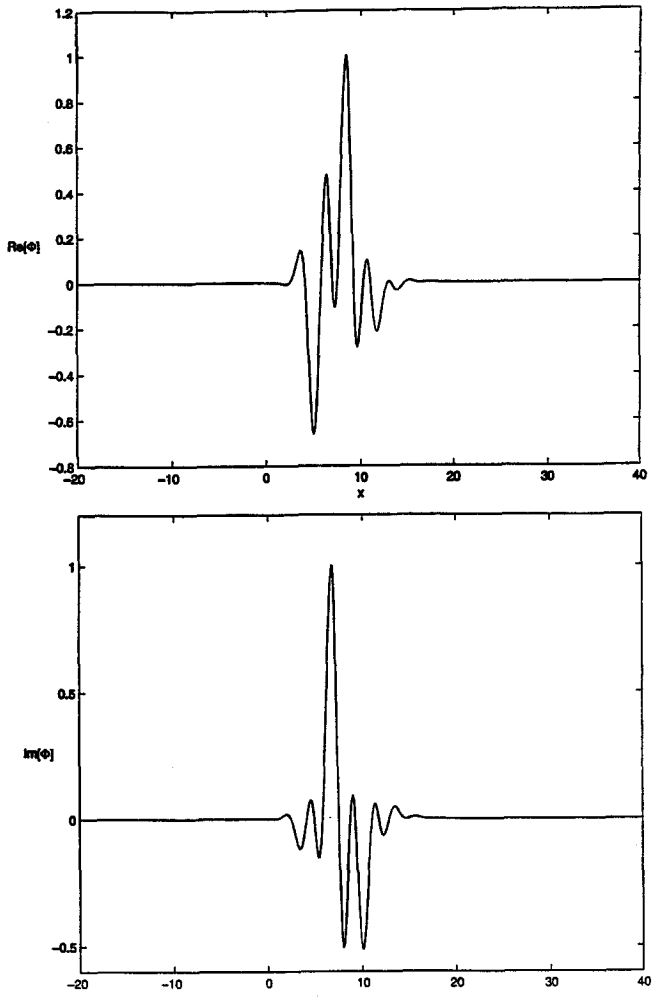

Fig. 12. – Global mode eigenfunction for Bubble A (global representation of $\alpha(X)$ and $\omega_0(X)$).

the bubble where the pressure gradient and the vorticity alternate in sign. Furthermore, the character of this instability is such that the intrinsic dynamics is synchronized and commonly extends over streamwise scales well beyond the isolated region of local absolute instability. As such, the global instability will give rise to a coherent array of vortex structures in the separation bubble which fluctuate in intensity with the discrete frequency of the global mode. Of course, the nonlinear saturation of this instability in real separated flows remains undefined and one can only speculate at this stage what is the ultimate fate of a separation bubble which is globally unstable.

It should be pointed out that other types of global modes are known to exist (*cf.* LeDizés *et al.*, 1996), but we have restricted this discussion to those specified by the criterion (12). The proposed symmetric base state, in fact, presents a good context to explore and contrast the different possible types of global modes, including weakly and strongly nonlinear states, but that is outside the scope of the present work.

6. Concluding remarks

Local and global stability considerations of model separation bubbles, constructed using a family of modified, separating Falkner-Skan velocity profiles, suggest that intrinsic, global dynamics can be expected in separation

bubbles when the peak back flow velocity exceeds about thirty percent of the ambient stream speed. This implies that smaller bubbles may be only marginally stable to a global (*i.e.*, streamwise) eigenmode, while separated regions of greater extent and depth are likely to be globally unstable. In the former case where the global mode is subcritical, injected disturbances of appropriate frequency and structure may be effective in triggering a global instability with consequent disruption of the stable bubble. This work suggests that experiments, either physical or numerical, to explore this possibility, and to identify the nonlinear dynamics of the globally unstable state, might be quite useful in revealing the potential for flow control of separated states. Experiments on pitching airfoils and dynamic stall indicate that separated regions containing reversed flows approaching forty percent of the ambient velocity exist (*cf.*, Crisler *et al.*, 1994). These specific experiments suggest that the rapid onset of some large scale dynamics occurs leading to the collapse of the separated region when the reversed flow approaches such strong magnitudes. Of course, the basic structure of the separating flow is time-dependent in this case. Hence the changing nature of the separated region may be a response to a larger scale motion impressed on the separating flow rather than the growth of an unstable global mode on a faster time scale. Nevertheless, the latter possibility cannot be ruled out based on the results of the present study.

The fact that larger separation bubbles in stationary, or slowly-varying flows, are likely to exhibit intrinsic global dynamics suggest that such regions are not necessarily regions of low stress, but rather contain coherent, synchronous motions that might be quite effective in facilitating vertical transport. Although preliminary evidence suggests that this might be the operative mechanism yielding the marked increase in sediment resuspension under upstream-propagating internal waves (*cf.*, Bogucki, Dickey & Redekopp, 1997), further studies are needed to either confirm or dispel this conjecture. Pauley *et al.* (1990) have studied numerically a separating flow in a channel where the separation is induced by a compact region of suction imposed on one side of the channel. This work reveals the onset of synchronous dynamics in the induced separation bubble when the applied suction (*i.e.*, the imposed adverse pressure gradient) exceeds a limiting value. There is no clear measure of the strength of the reversed flow in the bubble in Pauley *et al.* (1990) precluding a direct correlation with the predicted criteria for onset of global dynamics presented here. Nevertheless, the present work does provide generic, qualitative information for assessing when global instability might be expected in separating flows and elucidates what is the expected character of this instability in such flows. We have initiated numerical experiments to explore further the ideas put forward here.

Acknowledgements

This work was supported by the AFOSR under contract number F49620-92-J-0377 and by ONR under contract number N00014-95-1-0041. Some of the numerical work was performed through support from the San Diego Supercomputer Center.

APPENDIX

The transition between absolute and convective instability is studied for the hyperbolic-tangent shear layer in the presence of a plane wall. The results presented here extend those of Huerre and Monkewitz (1985) for an isolated free-shear layer to the case when a plane boundary is placed parallel to the shear layer on either the high-speed or the low-speed side. The boundary is assumed to be slip-free so far as the mean flow is concerned, but the both components of the disturbance velocity are assumed to vanish at the boundary since

the instability calculations are made using the same Orr-Sommerfeld solver employed to obtain the results reported in the main text.

The mean velocity profile of the parallel flow whose stability is examined is taken in the form

$$U(y) = 1 + r \tanh y, \tag{A.1}$$

where $U(y)$ has been scaled with the average speed of the two streams and the transverse coordinate y is scaled with one-half the vorticity thickness of the shear layer. The parameter r is the velocity ratio defined by

$$r = \frac{U_1 - U_2}{U_1 + U_2}, \tag{A.2}$$

where $U_{1,2}$ are the ambient velocity of the high-speed and low-speed streams, respectively. As is clear from (A.1), the shear layer is centered at $y = 0$ and the plane boundary is placed at either $y = +y_w$ or $y = -y_w$.

Instability calculations for $Re = 1000$ are shown in Figure A-1. Results for the absolute-convective transition boundary at this Reynolds number and without the presence of any confining boundaries are found to be within one percent of that reported by Huerre and Monkewitz (1985) based on an inviscid analysis. The instability is of absolute type whenever r exceeds the value along the curves shown in this figure. When the plane wall is placed on the low-speed side, there is an initial departure from the inviscid transition value to slightly lower values of r near $y_w = 14$, but the curve soon rises to progressively higher values of r as the wall is moved closer to the shear layer. When the wall is placed on the high-speed side, there is an initial departure from the inviscid transition value to lower values of r around $y_w = 11$. The transition value of r rises again as

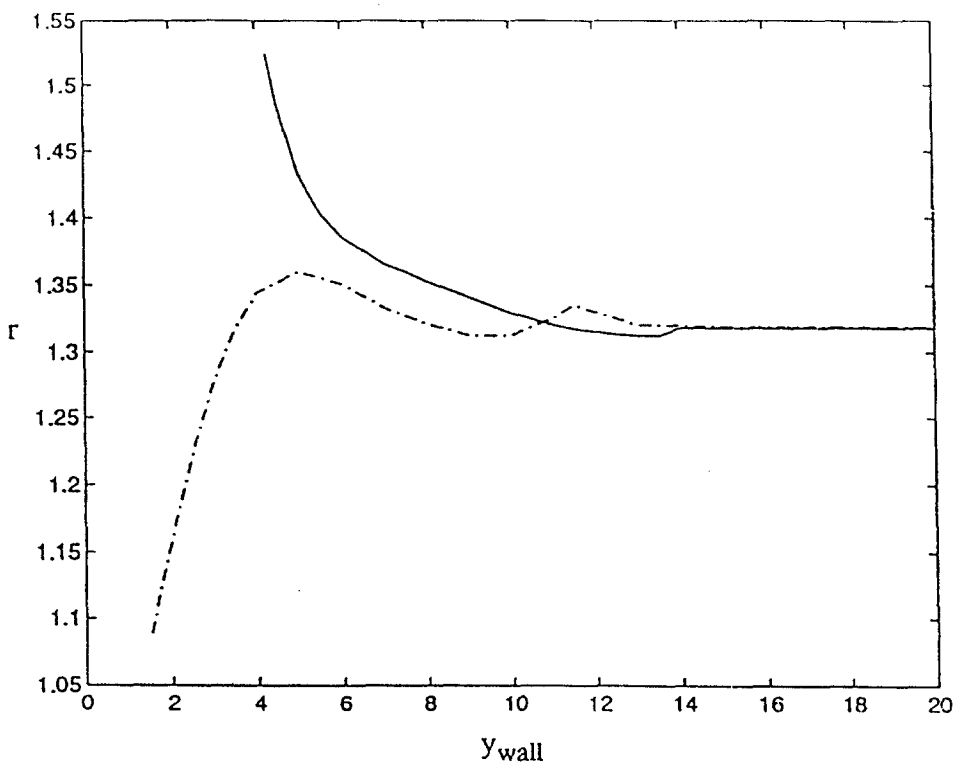

Fig. A-1. – Absolute-convective instability transition boundaries for the hyperbolic-tangent mixing layer in the vicinity of a wall. (——) wall placed on the low-speed side; (– – –) wall placed on the high-speed side.

the wall is moved toward the shear layer, however, it ultimately decreases as the wall is moved still closer to the mixing layer. It is evident though, for almost all positions of the wall, that the presence of a wall on the low-speed side makes the flow more convectively unstable while the presence of a wall on the high-speed side makes the flow more absolutely unstable.

REFERENCES

BOGUCKI D., DICKEY T. D., REDEKOPP L. G., 1997, Sediment resuspension and mixing by resonantly-generated internal solitary waves, *J. Phys. Ocean*, **27**, 1181-1196.

CHOMAZ J.-M., HUERRE P., REDEKOPP L. G., 1988, Bifurcations to local and global modes in spatially developing flows, *Phys. Rev. Lett.*, **60**, No. 1, 25-28.

CHOMAZ J.-M., HUERRE P., REDEKOPP L. G., 1990, The effect of nonlinearity and forcing on global modes, *New Trends in Nonlinear Dynamics and Pattern Forming Phenomena: The Geometry of Nonequilibrium* (P. Coullet & P. Huerre, eds.) NATO ASI Series B: Physics, **237**, pp. 259-274, Plenum Press, New York.

CHOMAZ J.-M., HUERRE P., REDEKOPP L. G., 1991, A frequency selection criteria in spatially developing flows, *Stud. Appl. Maths.*, **84**, 119-144.

CRISLER W., KROTHAPALLI A., LOURENCO L., 1994, PIV investigation of high speed flow over a pitching airfoil, *AIAA Paper 94-0533*, 32nd Aerospace Sciences Meeting, Reno, NV.

DAVEY A., 1973, A simple numerical method for solving Orr-Sommerfeld problems, *Quart. J. Mech. Appl. Math.*, **26**, 401-411.

DAVEY A., 1977, On the numerical solution of difficult eigenvalue problems, *J. Comput. Phys.*, **24**, 331-338.

DAVEY A., 1979, On the removal of the singularities from the Riccati method, *J. Comput. Phys.*, **30**, 137-144.

DOVGAL A. V., KOZLOV V. V., MICHALKE A., 1994, Laminar boundary layer separation: instability and associated phenomena, *Prog. Aerospace Sci.*, **3**, 61-94.

DRAZIN P. G., REID W. H., 1981, *Hydrodynamic Stability*, Cambridge University Press.

LE DIZÉS S., HUERRE P., CHOMAZ J.-M., MONKEWITZ P. A., 1996, Linear global modes in spatially-developing media. *Phil. Trans. Roy. Soc. London A*, **354**, 169-212.

LEES L., REEVES B. L., 1964, Supersonic separated and reattaching laminar flows: I. General theory and application to adiabatic boundary-layer/shock-wave interactions, *AIAA J.*, **2**, 1907-1920.

GASTER M., JORDINSON R., 1975, On the eigenvalues of the Orr-Sommerfeld equation, *J. Fluid Mech.*, **72**, 121-133.

HUERRE P., MONKEWITZ P. A., 1985, Absolute and convective instabilities in free shear layers, *J. Fluid Mech.*, **159**, 151-168.

MONKEWITZ M., 1978, Analytic pseudo-orthogonalization methods for linear-two point boundary value problems illustrated by the Orr-Sommerfeld equation, *J. Appl. Math & Phys.*, **29**, 861-870.

MONKEWITZ P. A., HUERRE P., CHOMAZ J.-M., 1993, Global linear stability analysis of weakly non-parallel shear flows, *J. Fluid Mech.*, **251**, 1-20.

O'MEARA M. M., MUELLER T. J., 1987, Laminar separation bubble characteristics on an airfoil at low Reynolds numbers, *AIAA J.*, **25**, 1033-1041.

PAULEY L. L., MOIN P., REYNOLDS W. C., 1990, The structure of two-dimensional separation, *J. Fluid Mech.*, **220**, 397-411.

SCHLICHTING H., 1968, *Boundary Layer Theory*, Mc-Graw-Hill, Sixth Edition, p. 150.

WARD J. W., 1963, The behaviour and effects of laminar separation bubbles on airfoils in incompressible flow, *J. Roy. Aero. Soc.*, **67**, 783-790.

WAZZAN A. R., TAGHAVI H., KELTNER G., 1974, Effect of boundary-layer growth on stability of incompressible flat plate boundary layer with pressure gradient, *Phys. Fluids*, **17**, 1655-1660.

(Manuscript received July 15, 1996;
revised October 06, 1997;
accepted October 16, 1997.)